

# *Coherence of the AMOC over the Subpolar North Atlantic on interannual to multiannual time scales*

Article

Published Version

Creative Commons: Attribution 4.0 (CC-BY)

Open Access

Petit, T. ORCID: <https://orcid.org/0000-0002-7922-9363>,  
Robson, J. ORCID: <https://orcid.org/0000-0002-3467-018X>,  
Ferreira, D. ORCID: <https://orcid.org/0000-0003-3243-9774>,  
Yeager, S. and Evans, D. G. (2025) Coherence of the AMOC  
over the Subpolar North Atlantic on interannual to multiannual  
time scales. *Geophysical Research Letters*, 52 (9).  
e2025GL115171. ISSN 1944-8007 doi:  
10.1029/2025GL115171 Available at  
<https://centaur.reading.ac.uk/122516/>

It is advisable to refer to the publisher's version if you intend to cite from the work. See [Guidance on citing](#).

To link to this article DOI: <http://dx.doi.org/10.1029/2025GL115171>

Publisher: American Geophysical Union

All outputs in CentAUR are protected by Intellectual Property Rights law, including copyright law. Copyright and IPR is retained by the creators or other copyright holders. Terms and conditions for use of this material are defined in the [End User Agreement](#).

[www.reading.ac.uk/centaur](http://www.reading.ac.uk/centaur)

## **CentAUR**

Central Archive at the University of Reading

Reading's research outputs online

# Geophysical Research Letters<sup>®</sup>



## RESEARCH LETTER

10.1029/2025GL115171

### Key Points:

- The density at which the subpolar overturning streamfunction is maximum is a key precursor of the mid-latitude overturning strength
- The density anomaly propagates from the subpolar gyre to 45°N by following the western boundary within a year
- The density anomaly over the subpolar gyre is atmospherically driven by changes in buoyancy and wind forcings

### Supporting Information:

Supporting Information may be found in the online version of this article.

### Correspondence to:

T. Petit,  
tillys.petit@noc.ac.uk

### Citation:

Petit, T., Robson, J., Ferreira, D., Yeager, S., & Evans, D. G. (2025). Coherence of the AMOC over the subpolar North Atlantic on interannual to multiannual time scales. *Geophysical Research Letters*, 52, e2025GL115171. <https://doi.org/10.1029/2025GL115171>

Received 30 JAN 2025

Accepted 11 APR 2025

### Author Contributions:

**Conceptualization:** T. Petit, J. Robson

**Investigation:** T. Petit, J. Robson, D. Ferreira, S. Yeager, D. G. Evans






**Resources:** J. Robson, S. Yeager

**Visualization:** T. Petit

**Writing – original draft:** T. Petit

**Writing – review & editing:** T. Petit, J. Robson, D. Ferreira, S. Yeager, D. G. Evans

## Coherence of the AMOC Over the Subpolar North Atlantic on Interannual to Multiannual Time Scales

T. Petit<sup>1,2</sup> , J. Robson<sup>2</sup> , D. Ferreira<sup>3</sup> , S. Yeager<sup>4</sup> , and D. G. Evans<sup>1</sup> 

<sup>1</sup>National Oceanography Centre, Southampton, UK, <sup>2</sup>National Centre for Atmospheric Science, Department of Meteorology, University of Reading, Reading, UK, <sup>3</sup>Department of Meteorology, University of Reading, Reading, UK, <sup>4</sup>National Center for Atmospheric Research, Boulder, CO, USA

**Abstract** Direct measurements of the Atlantic Meridional Overturning Circulation (AMOC) are necessary to understand its evolution in a context of climate change. International programs monitored its recent evolution at different latitudes. However, the AMOC coherence over the North Atlantic remains unclear. Here, we explore the potential of the Overturning in the Subpolar North Atlantic Programme (OSNAP) array to inform us on mid-latitude AMOC strength on interannual-to-multiannual timescales in two high-resolution coupled models. We find that the AMOC strength measured at OSNAP is not related to the variability of the AMOC strength at mid-latitudes. Instead, our study reveals that the density at which the maximum overturning occurs at OSNAP is a key precursor of the mid-latitude AMOC strength. The causal relationship between AMOC density at the OSNAP array and AMOC strength at 45°N is linked to an atmospherically driven shoaling of isopycnal surfaces that propagates along the western boundary in a year.

**Plain Language Summary** Warm and salty water flows northward at surface into the high latitudes of the North Atlantic. This water is made heavier as it becomes colder and fresher and forms a return southward flow at depth. Direct measurements of this so-called Atlantic Meridional Overturning Circulation (AMOC) have been ongoing in the subtropical North Atlantic since 2004, and more recently in the subpolar North Atlantic. These measurements tell us that the AMOC in these two geographically adjacent regions do vary from daily to interannual timescales. However, the coherence of the varying AMOC between these two observational systems remains unclear. Our study shows that density changes in the subpolar North Atlantic propagate around the boundary of the subpolar North Atlantic within 1 year to modify the AMOC strength at mid-latitudes. We further show that these density changes are linked to the dominant atmospheric mode of variability known as the North Atlantic Oscillation (NAO). The NAO affects sea level pressure, altering the wind stress and buoyancy exchange at the sea surface, therefore changing surface density. These results will help inform how we design future ocean observing systems.

## 1. Introduction

The Atlantic Meridional Overturning Circulation (AMOC) is a key component of global climate through its role in redistributing heat, freshwater and carbon between the tropics and high latitudes in the North Atlantic. Since 2004, the RAPID array has continuously measured the AMOC at 26°N, revealing large variability in the subtropical AMOC from daily to annual timescales (Johns et al., 2023; McCarthy et al., 2015). More recently, the Overturning in the Subpolar North Atlantic Programme (OSNAP) array was deployed in 2014 to provide continuous measurements of volume transport across the subpolar gyre (Fu et al., 2023; Lozier et al., 2019). The array consists of two sections: OSNAP East from the Scottish shelf to the southeastern tip of Greenland and OSNAP West at the entrance of the Labrador Sea. The OSNAP array revealed the key role of dense water formation between the Greenland-Scotland Ridge and the OSNAP East array for the mean and monthly variability of the subpolar AMOC (Fu et al., 2024; Petit et al., 2020). However, the latitudinal AMOC coherence between the subpolar and subtropical gyres remains unclear, and the respective roles of the Irminger-Iceland and Labrador seas for the AMOC variability further south have been called into question.

The latitudinal coherence of the AMOC is believed to be time-scale dependant. On decadal timescales, modeling studies have showed that AMOC anomalies generated at subpolar latitudes propagate coherently to subtropical latitudes, with an emphasis on the role of the Labrador Sea as the center of action for generating AMOC anomalies (Bailey et al., 2005; Böning et al., 2006; Danabasoglu et al., 2012; Yeager et al., 2021). The propagation is

© 2025. The Author(s).

This is an open access article under the terms of the [Creative Commons Attribution License](#), which permits use, distribution and reproduction in any medium, provided the original work is properly cited.

explained by either advective processes (Buckley et al., 2012; Jackson et al., 2016; Marotzke & Klinger, 2000) or boundary waves (Biaostoch et al., 2008; Eden & Willebrand, 2001; Marshall & Johnson, 2013). While these studies describe a southward propagation of the AMOC anomaly, other modeling studies have shown that high latitude AMOC variability lags mid-latitude AMOC changes at multidecadal timescales (Kwon & Frankignoul, 2014), suggesting that the overturning variability observed at OSNAP is a response to AMOC anomalies generated further south.

On interannual timescales, the latitudinal coherence of the overturning cell is shown to breakdown between subpolar and subtropical latitudes (Biaostoch et al., 2008; Bingham et al., 2007; Xu et al., 2014), which suggests a lack of AMOC consistency between the OSNAP sections and 45°N. However, modeling studies show a meridional connection between the subpolar and subtropical gyres associated with Lower North Atlantic Deep Water (LNADW) transport (Kostov et al., 2021, 2022; Zou et al., 2020). Kostov et al. (2022) explained this meridional connectivity by the fast propagation of density anomalies from the Labrador Sea to the subtropical gyre via boundary trapped waves. Furthermore, Menary et al. (2020) showed that density anomalies propagating along the boundary of the subpolar gyre drive AMOC changes at the OSNAP sections in the coupled model HadGEM3-GC3.1-MM. While no coherence has been detected when linking the subpolar and subtropical AMOC variability during the short period of overlap between the OSNAP and RAPID arrays (Frajka-Williams et al., 2023; Jackson et al., 2022), observations do support a meridional connectivity of LNADW between these latitudes at interannual and sub-annual timescales (Frajka-Williams et al., 2016; Smeed et al., 2014).

Taken together, these studies raise questions about: (a) the latitudinal coherence of the AMOC at interannual timescale and, more precisely, the potential to use the OSNAP array to predict the AMOC further south, (b) the role of density anomalies propagating along the boundary of the subpolar gyre for the AMOC coherence, and (c) the extent to which the connectivity is driven by common atmospheric forcing (Fraser et al., 2025; Kostov et al., 2021; Zou et al., 2020) or by a continued propagation of the boundary signal (Hodson & Sutton, 2012). To address these questions, we use two high-resolution coupled models to investigate the relationships between AMOC variability at the OSNAP array and 45°N focusing on interannual-to-multiannual timescales.

## 2. Materials and Methods

### 2.1. High-Resolution Coupled Models

We use two high-resolution coupled models to evaluate the latitudinal coherence of the AMOC, HadGEM3-GC3.1-HH and CESM1.3-HR. HadGEM3-GC3.1-HH was developed as part of the High-Resolution Model Intercomparison Project protocol for CMIP6 (Haarsma et al., 2016). It has an atmosphere resolution of 50 km and an ocean resolution of 8 km at mid-latitudes, with 75 levels in the vertical (Roberts et al., 2020). We use the 1950s control simulation of HadGEM3-GC3.1-HH that was subject to constant 1950s external forcings and, after a spin-up of 30 years, integrated for 100 years. CESM1.3-HR has a nominal atmosphere resolution of 0.25° and a nominal ocean resolution of 0.1° with 62 levels in the vertical (Chang et al., 2020). We use the preindustrial control simulation of CESM1.3-HR that was initialized from climatological 1850s conditions and integrated for 500 years. Over the 500 years of the simulation, we used the nominal years 250–480 to avoid the instability of the spin-up period. We will refer to these as HH and CESM, respectively.

These two models were chosen to evaluate the latitudinal coherence of the AMOC because of their consistency with measured AMOC at subpolar (Petit, Robson, et al., 2023; Yeager et al., 2021) and subtropical latitudes (Chang et al., 2020; Roberts et al., 2019), and because they broadly resolves narrow boundary currents (Figure S1 and Text S1 in Supporting Information S1).

### 2.2. Estimation of Overturning Streamfunction

The AMOC streamfunction ( $\psi_y$ ) is defined as the integrated transport across a section in density space, with the AMOC strength ( $\psi_y^{\max}$ ) being the maximum of the AMOC streamfunction ( $1 \text{ Sv} = 10^6 \text{ m}^3 \text{ s}^{-1}$ ). Here we estimate the AMOC strength in density coordinates, with density referenced to the surface:

$$\psi_y^{\max}(t) = \max_{\sigma} [\psi_y(t, \sigma)] = \max_{\sigma} \left[ \int_{\sigma_{\text{bot}}}^{\sigma} \int_{x_w}^{x_e} v(x, \sigma, t) dx d\sigma \right],$$

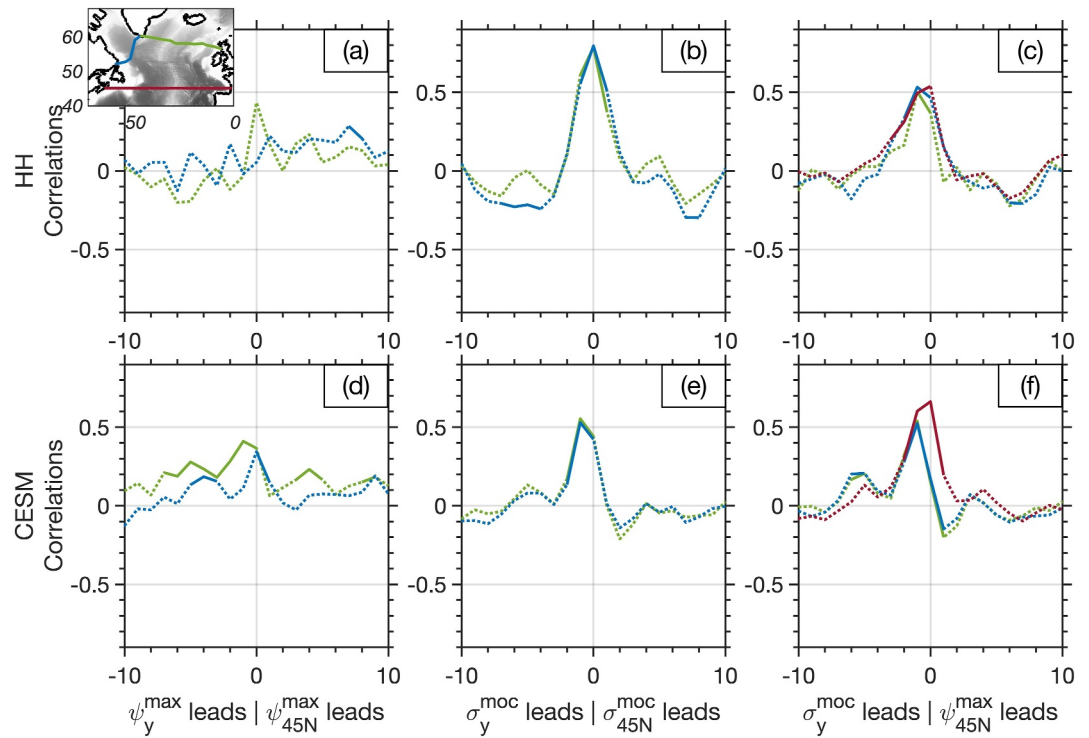


**Figure 1.** Lead-lag correlations (year) between (a, d) the overturning strength ( $\psi_y^{\max}$ ) at 45°N and at Overturning in the Subpolar North Atlantic Programme (OSNAP) East and OSNAP West, (b, e) the Atlantic Meridional Overturning Circulation (AMOC) density ( $\sigma_y^{\text{moc}}$ ) at 45°N and at OSNAP East and OSNAP West, and (c, f) the overturning strength at 45°N and the AMOC density at OSNAP East, OSNAP West and 45°N for the (a–c) HH and (d–f) CESM models. The subscript “y” denotes OSNAP East (green lines), OSNAP West (blue lines), and 45°N (red lines), with the location of each section indicated in the inserted map. Plain (dashed) lines indicate (non-)significant correlations.

where  $v$  is the velocity normal to the section considered,  $\sigma$  is density,  $t$  is time, and  $x$  is longitude with  $x_e$  and  $x_w$  being the eastern and western end points of a section at nominal latitude  $y$ , respectively. The density at the maximum of the AMOC streamfunction is called AMOC density,  $\sigma_y^{\text{moc}}(t)$ .

The AMOC streamfunction was estimated at three sections: 45°N, OSNAP East, and OSNAP West (Figure 1). Because latitude is not constant for the latter two sections, meridional and zonal velocities were extracted as close as possible to the observed lines and used to estimate a velocity normal to the sections. No compensation due to the net throughflow is applied at these sections, following Menary et al. (2020).

Although the AMOC streamfunction is estimated from monthly outputs, the annually averaged  $\psi_y^{\max}$  and  $\sigma_y^{\text{moc}}$  were deduced from annually averaged AMOC streamfunction. The time series of  $\psi_y$ ,  $\psi_y^{\max}$  and  $\sigma_y^{\text{moc}}$  were linearly detrended with time, and the significance of the correlations between these time series were estimated based on a Student's  $t$ -test at the  $p < 0.05$  level.

### 3. Results

#### 3.1. Meridional Coherence of the Overturning

The relationship between the AMOC strength at OSNAP East, OSNAP West and 45°N is first investigated in Figures 1a and 1d. The correlations show that the AMOC strength at either OSNAP East or OSNAP West is not strongly related to that at 45°N with or without lag. The lack of latitudinal coherence in AMOC strength across the North Atlantic subpolar gyre is consistent between the two models and reveals that the AMOC strength measured at the OSNAP sections is not related to the variability of the mid-latitude AMOC strength at interannual-to-multiannual timescales.

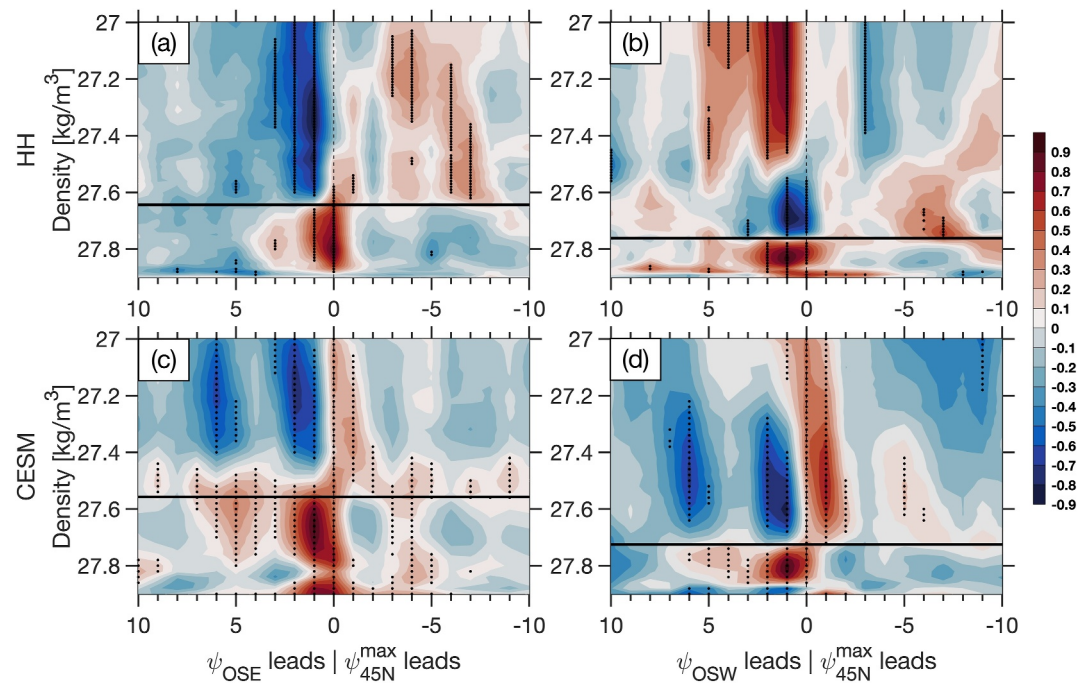


**Figure 2.** Lead-lag correlations (year) between the overturning strength at 45°N ( $\psi_{45N}^{max}$ ) and the overturning streamfunctions at (a, c) Overturning in the Subpolar North Atlantic Programme (OSNAP) East ( $\psi_{OSE}$ ) and (b, d) OSNAP West ( $\psi_{OSW}$ ) for the (a, b) HH and (c, d) CESM models. Black plain lines indicate the mean  $\sigma_y^{moc}$  at each section. Black dots indicate significant correlations.

However, a strong relationship is found between the density at which the maximum overturning occurs across the three sections (Figures 1b and 1e). The AMOC density is well correlated on annual timescales between OSNAP East, OSNAP West and 45°N in both models, which are significant at the  $p < 0.05$  level. The highest correlation is found at 0-year lag for the HH model, where the AMOC density change at the two OSNAP sections accounts for ~64% of the variability of that at 45°N (correlation coefficient of 0.80), and at 1-year lag for the CESM model, where the AMOC density change at the two OSNAP sections accounts for ~30% of that at 45°N (correlation coefficient of 0.53).

The impact of the AMOC density on the AMOC strength is now examined in Figures 1c and 1f, which shows the lead/lag correlation coefficients between the AMOC strength at 45°N and the density of the maximum overturning streamfunction at the three sections. For both models, the strong correlation at 1-year lag is statistically significant and implies that an AMOC densification at the OSNAP sections leads to a rapid intensification of the AMOC strength at 45°N. More precisely, a change in  $\sigma_y^{moc}$  at the OSNAP sections explains ~30% of the inter-annual variability in AMOC strength at 45°N. An AMOC densification at 45°N is also associated with an intensification of the AMOC strength at the same section (red lines), underlining the strong relationship between the density and strength of the AMOC at 45°N. Thus, the AMOC density at each of the OSNAP sections are key precursors of the mid-latitude AMOC strength.

A closer inspection of the relationship between AMOC density and AMOC strength reveals that changes in AMOC density are associated with changes in the density range of the AMOC streamfunction. Figures 2a and 2c shows the lead/lag correlation coefficients at different density between the mid-latitude AMOC strength and the values of the OSNAP East overturning streamfunction at that density. The dipole in correlation at 1 year lag indicates that an intensification of the AMOC strength at 45°N is led by a shift in the overturning streamfunction toward higher density at OSNAP East. In other words, a densification of the water column at OSNAP East does not lead to an intensification of the AMOC strength at that section, but leads to an intensification of the AMOC strength further south, at 45°N. This relationship, which is consistent across models, is also found downstream when considering the correlation in density space between the AMOC strength at 45°N and the AMOC streamfunction at OSNAP West (Figures 2b and 2d).



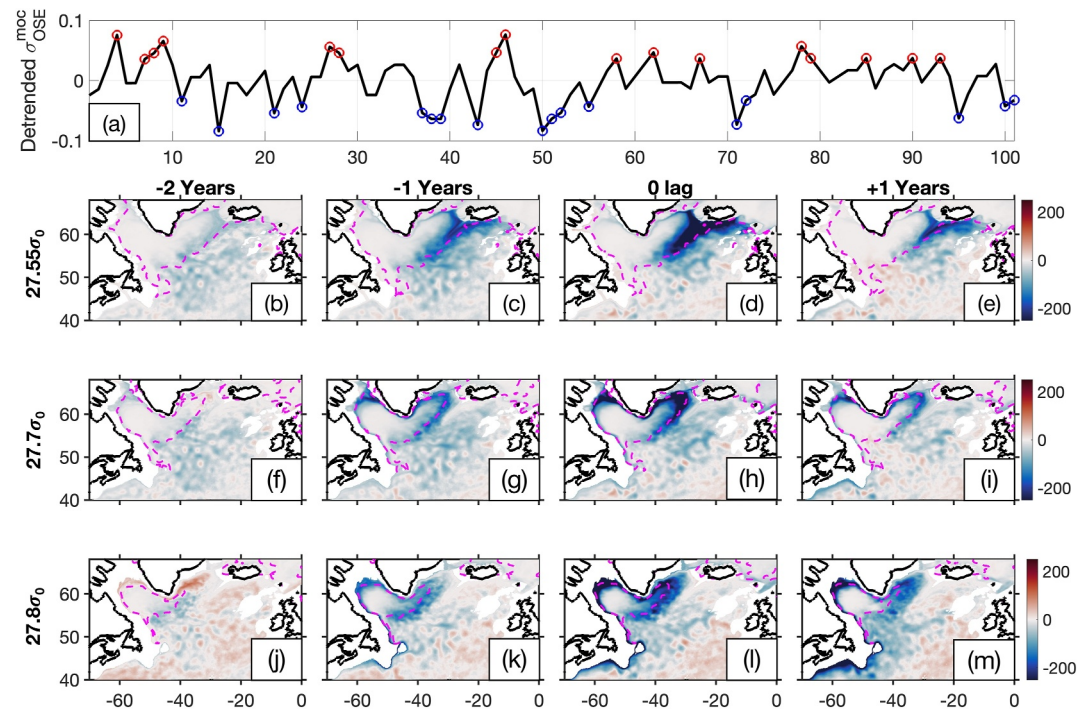


**Figure 3.** (a) Annual variability of the detrended  $\sigma_{\text{OSE}}^{\text{moc}}$  at Overturning in the Subpolar North Atlantic Programme East in the HH model. Red and blue circles indicate years of relatively dense and light  $\sigma_{\text{OSE}}^{\text{moc}}$  used for the composite analysis ( $\pm 1$  standard deviation of the  $\sigma_{\text{OSE}}^{\text{moc}}$  annual variability), respectively. (b–m) Lead/lag difference of composite anomalies in the depth of the isopycnals (b–e)  $27.55\sigma_0$ , (f–i)  $27.7\sigma_0$ , and (j–m)  $27.8\sigma_0$ . Negative differences indicate a shallower isopycnal during years of dense  $\sigma_{\text{OSE}}^{\text{moc}}$ . Purple dashed lines indicate the isopycnals (b–e)  $27.55\sigma_0$ , (f–i)  $27.7\sigma_0$ , and (j–m)  $27.8\sigma_0$  at surface in wintertime (JFM) during years of dense  $\sigma_{\text{OSE}}^{\text{moc}}$ .

### 3.2. Propagation of AMOC Densification Over the Subpolar Gyre

To assess the mechanisms explaining the causal relationship between AMOC densification at the OSNAP sections and AMOC strengthening at  $45^\circ\text{N}$ , we use a composite analysis for periods of dense and light AMOC density at OSNAP East (Figure 3a, Figure S3a in Supporting Information S1). We use the AMOC density at OSNAP East instead of the other two sections to investigate the propagation of anomalies from the eastern subpolar gyre to  $45^\circ\text{N}$ . The differences between the two composites (i.e., dense minus light  $\sigma_{\text{OSE}}^{\text{moc}}$ ) are evaluated in the following.

The composite analysis is first applied to the density field at  $45^\circ\text{N}$  (Figure S2 in Supporting Information S1). A year after an AMOC densification at OSNAP East, the western boundary of the section at  $45^\circ\text{N}$  becomes significantly denser west of  $45^\circ\text{W}$  and lighter east of  $45^\circ\text{W}$  in the upper 1,000-m depths, which includes all isopycnals lighter than  $\sim 27.8 \text{ kg m}^{-3}$ . The density field over the eastern boundary of the section, however, remains largely unchanged. This indicates that positive density anomalies along the western boundary leads to an asymmetry in the slope of isopycnal surfaces between the boundaries at  $45^\circ\text{N}$ , resulting in an increase in shear via thermal wind balance (Buckley & Marshall, 2016; Hirschi & Marotzke, 2007) and thus a strengthening of the mid-latitude AMOC (Figure 1f).

To explore the role of oceanic processes linking the anomalies in AMOC density between the sections, we next apply the composite analysis to the interface depth of isopycnals localized in the AMOC lower limb. We first focus on  $\sigma_0 = 27.8$  in the HH model, with Figures 3b–3m showing the differences between the two depth composites. The composite analysis reveals that a dense  $\sigma_{\text{OSE}}^{\text{moc}}$  is related to a shoaling of  $\sigma_0 = 27.8$  in the interior of the Irminger Sea, along the boundary of the Labrador Sea, and south of Flemish Cap at  $45^\circ\text{N}$  (Figure 3l). At these locations,  $\sigma_0 = 27.8$  is more than 200 m shallower during years of dense  $\sigma_{\text{OSE}}^{\text{moc}}$  as compared to years of light  $\sigma_{\text{OSE}}^{\text{moc}}$ . The shoaling of  $\sigma_0 = 27.8$  starts 2 years before an AMOC densification at OSNAP East, with a weak shoaling in the interior of the Irminger Sea and south of Greenland (Figure 3j). Later, the depth anomaly of  $\sigma_0 = 27.8$

intensifies and propagates in the interior of the Irminger Sea and along the western boundary (Figure 3k). A year after an AMOC densification at OSNAP East, the depth anomaly starts to weaken in the interior of the Irminger Sea but remains relatively strong along the western boundary until 45°N (Figure 3m). The propagation of isopycnal depth anomaly from the subpolar gyre to 45°N is further highlighted in Figure S4 in Supporting Information S1 showing that the shoaling of  $\sigma_0 = 27.8$  starts in the winter of 1-year lag and reaches 45°N as early as May-June of the same year.

The link in AMOC densification between the sections is thus explained by a shoaling of dense isopycnal surfaces over the subpolar gyre that propagate to 45°N along the western boundary, as opposed to via interior pathways, within only a few months. At 45°N, this shoaling steepens the isopycnals along the western boundary, resulting in a strengthening of the mid-latitude AMOC strength. The propagation of depth anomalies along the western boundary is also found in the CESM model (Figures S3j–S3m in Supporting Information S1), although the shoaling of the isopycnal starts at 0-year lag in this model instead of 2-year lag, suggesting a faster propagation of the anomaly due to an overall deeper isopycnal in the CESM model as compared to the HH model.

### 3.3. Generation of AMOC Densification Over the Subpolar Gyre

We next evaluate the drivers of AMOC densification over the subpolar gyre. The propagation of isopycnal depth anomalies can be tracked from the subpolar gyre to 45°N within a few months, but the location where these anomalies are first generated over the subpolar gyre is more difficult to ascertain. Shoaling of isopycnal surfaces occurs simultaneously over both the Irminger and Labrador seas during the winter preceding an AMOC densification (Figure S4 in Supporting Information S1). This suggests that the densification is either (a) generated over these areas together by a spatially coherent atmospheric signal or (b) that its propagation from one basin to the next is quicker than a month.

Moreover, the location of isopycnal depth anomalies over the subpolar gyre varies when the composite analysis is applied to isopycnal surfaces other than  $\sigma_0 = 27.8$ . When applied to  $\sigma_0 = 27.7$ , the shoaling is localized over the eastern boundary of the Irminger Sea in the HH model (Figures 3f–3i) and over the Reykjanes Ridge in the CESM model (Figures S3f–S3i in Supporting Information S1). When applied to  $\sigma_0 = 27.55$ , the shoaling is localized over the Reykjanes Ridge in the HH model (Figures 3b–3e) and over the Iceland Basin in the CESM model (Figures S3b–S3e in Supporting Information S1). These locations match areas where the associated isopycnal outcrops at surface in winter (purple lines). Thus, although the shoaling of all isopycnal surfaces propagates along the western boundary of the subpolar gyre, their center of action over the subpolar gyre depends on the location at which the isopycnal outcrops at surface (i.e., eastern subpolar gyre for light water masses and western subpolar gyre for dense water masses), which suggests that the shoaling of isopycnal surfaces is mainly driven by surface processes.

To investigate the atmospheric mechanisms leading to an AMOC densification over the subpolar gyre, the composite analysis is applied to the winter sea level pressure (SLP), net heat flux, vertical Ekman velocity and surface density (Figure 4, Figure S5 in Supporting Information S1). The two models show anomalously low SLP over the northern subpolar gyre, to the north of the OSNAP line, from 1 year before an AMOC densification at OSNAP East. The anomaly in SLP, like a North Atlantic Oscillation (NAO) pattern, drives stronger wind stress curl that leads to upward Ekman velocity over the eastern subpolar gyre, which is particularly intense at 0-year lag. The anomaly in SLP also enhances heat loss over most of the subpolar gyre, and most particularly over the western subpolar gyre. Although we do not investigate the NAO drivers, we note that these conditions develop alongside a densification of surface water along the Gulf Stream Extension region, and that temperature anomalies at the Gulf Stream front have been shown to influence winter NAO (Famooss Paolini et al., 2022).

An AMOC densification over the subpolar gyre is therefore mainly driven by positive NAO conditions, resulting in intense Ekman suction over the eastern subpolar gyre and intense heat loss over the western subpolar gyre. Although an exact partitioning of the eastern and western contributions to a subpolar AMOC densification is difficult to establish without more dedicated model experiments than available here, the results can be interpreted following two hypotheses: either Ekman suction drives AMOC densification over the eastern subpolar gyre, or heat loss drives AMOC densification over the western subpolar gyre. These two hypotheses are not necessarily competitive but most likely act in concert to drive a simultaneous AMOC densification over both the Irminger and Labrador seas, which then propagates to 45°N in few months.



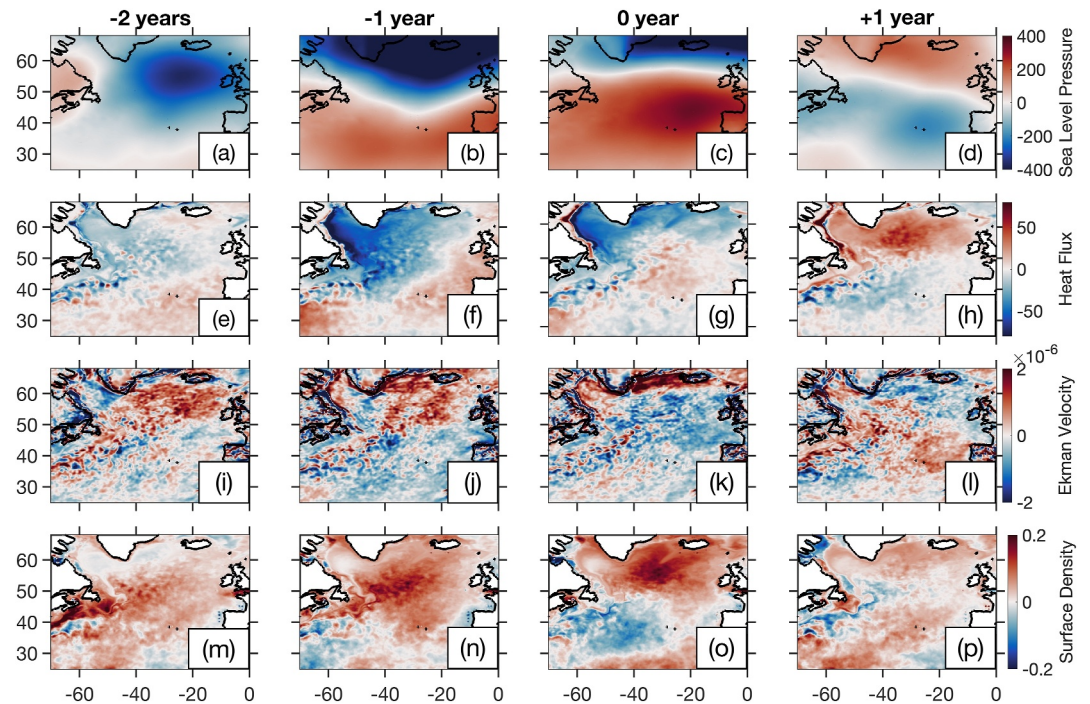


**Figure 4.** Lead/lag composite anomalies in winter (a–d) Sea Level Pressure (Pa), (e–h) Heat Flux ( $\text{W/m}^2$ ), (i–l) vertical Ekman velocity ( $\text{m/s}$ ), and (m–p) surface density ( $\text{kg/m}^3$ ) in the HH model. Negative anomalies in heat flux indicate stronger heat loss during years of dense  $\sigma_{\text{OSE}}^{\text{moc}}$ . Positive anomalies in Ekman velocity and surface density indicate stronger upward velocity and densification during years of dense  $\sigma_{\text{OSE}}^{\text{moc}}$ .

#### 4. Discussion and Conclusions

Our analysis investigates the links between the AMOC annual variability at the OSNAP sections and at  $45^\circ\text{N}$  in two high-resolution climate models. We show that the mid-latitude AMOC strength is strongly related to the AMOC density found at OSNAP 1 year before. However, the AMOC strength measured at OSNAP does not lead mid-latitude AMOC variability on annual timescales. Therefore, the OSNAP arrays potential to inform us on the strength of the mid-latitude AMOC lies in its measurement of the AMOC density at high latitudes. This suggests that observing the AMOC density at only one of the two OSNAP sections could suffice to monitor changes in the mid-latitude AMOC. Hence, such relationships should be further explored when considering the future design of the AMOC observing system.

A change in AMOC density at OSNAP is associated with a shift in the density of the overturning streamfunction and thus to the shoaling of isopycnal surfaces that propagates from the subpolar gyre to  $45^\circ\text{N}$  along the western boundary within few months. At  $45^\circ\text{N}$ , the resultant steeper isopycnal surfaces along the western boundary modify the zonal density gradient at  $45^\circ\text{N}$ , impacting the mid-latitude AMOC strength. The rapid propagation of density anomalies along the western boundary can be explained by topographic waves, as opposed to interior Rossby waves (Johnson et al., 2019; Marshall & Johnson, 2013), as suggested by Kostov et al. (2022) to explain the connection of LNADW transport between subpolar and subtropical gyres. As such, these results indicate that the southward advection of transport anomalies from OSNAP latitudes (Biló & Johns, 2019; Chomiak et al., 2022; Curry et al., 1998; Petit, Lozier, et al., 2023; Zhai et al., 2021) is not the prevailing metric to inform us on changes in the mid-latitude AMOC strength.

The mechanisms generating an AMOC densification over the subpolar gyre are atmospherically driven by changes in NAO conditions and possibly other atmospheric modes of variability (Thornton et al., 2023). Positive NAO conditions drive upward Ekman velocities over the eastern subpolar gyre and stronger heat loss over the western subpolar gyre. Positive NAO conditions can also lead to densification of surface waters through southward Ekman transport (Deser et al., 2009; Khatri et al., 2022). The respective roles of the eastern and western subpolar gyre in generating these anomalies at  $45^\circ\text{N}$  is difficult to ascertain. Indeed, although the key role

of the NAO for AMOC variability was found in previous studies (Danabasoglu, 2008; Getzlaff et al., 2005; Khatri et al., 2022), the dominant source location for the generation of anomalies varies between the Labrador Sea (Danabasoglu et al., 2012) and Irminger Sea (Megann et al., 2021). Here, we posit that changes in AMOC density are not generated within a defined area or basin but, instead, that buoyancy forcing over the western subpolar gyre and wind forcing over the eastern subpolar gyre act in concert to form density anomalies at subpolar latitudes. Removing the Ekman component of the overturning at one of the OSNAP sections (Khatri et al., 2022) or developing dedicated sensitivity experiments of decoupled models with, for example, varying wind forcing and fixed buoyancy forcing (e.g., Markina et al., 2024; Polo et al., 2014) would be required to quantify the exact partitioning of the eastern and western contributions.

Finally, we stress that the mechanisms driving an AMOC densification are time-scale dependant. Focusing on interannual-to-multiannual timescales, our study shows a latitudinal coherence in the AMOC density that is driven by a combination of wind and buoyancy forcing over the subpolar gyre. On multidecadal timescales, Yeager et al. (2021) showed that the AMOC strength at 45°N is related to subpolar AMOC densification but highlighted that the AMOC densification is mainly driven by buoyancy forcing over the Labrador Sea, which is supported by Böning et al. (2023). Therefore, these studies suggest that the relative contribution of buoyancy forcing over the western subpolar gyre becomes more important for AMOC densification than the wind forcing mechanism over the eastern subpolar gyre on climatic timescales.

## Data Availability Statement

The model outputs used in this study are freely available at <https://www.wdc-climate.de/ui/cmip6?input=CMIP6.HighResMIP.MOHC.HadGEM3-GC31-HH.control-1950> for HadGEM3-GC3.1-HH (Malcolm, 2018) and at <https://rda.ucar.edu/datasets/d651029/> for CESM1.3-HR (Castruccio et al., 2025).

## Acknowledgments

We wish to thank M. Susan Lozier for her insightful feedback on the study. We also thank the two reviewers for their helpful comments on the manuscript. T.P., D.F., and J.R. were supported by NERC through the SNAP-DRAGON (NE/T013494/1) project. JR was also supported by NERC through the WISHBONE (NE/T013516/1), CANARI (NE/W004984/1), and ALPACA (NE/Y005279/1) projects. J.R. was additionally funded by the UKRI (10039018) as part of the EPOC project (Explaining and Predicting the Ocean Conveyor; Grant 101059547). Views and opinions expressed are however those of the authors only and do not necessarily reflect those of the European Union. Neither the European Union nor the granting authority can be held responsible for them. S.Y. acknowledges support from the US National Science Foundation (NSF) Grant GEO-OCE 2040020. NCAR is a major facility sponsored by NSF under Cooperative Agreement 1852977. D.G.E. was funded by NERC research Grant NE/R015953/1.

## References

- Bailey, D. A., Rhines, P. B., & Häkkinen, S. (2005). Formation and pathways of North Atlantic deep water in a coupled ice–ocean model of the Arctic–North Atlantic Oceans. *Climate Dynamics*, 25(5), 497–516. <https://doi.org/10.1007/s00382-005-0050-3>
- Biaostoch, A., Böning, C. W., Getzlaff, J., Molines, J.-M., & Madec, G. (2008). Causes of interannual–decadal variability in the meridional overturning circulation of the midlatitude North Atlantic Ocean. *Journal of Climate*, 21(24), 6599–6615. <https://doi.org/10.1175/2008JCLI2404.1>
- Biló, T. C., & Johns, W. E. (2019). Interior pathways of Labrador Sea water in the North Atlantic from the Argo perspective. *Geophysical Research Letters*, 46(6), 3340–3348. <https://doi.org/10.1029/2018GL081439>
- Bingham, R. J., Hughes, C. W., Roussinov, V., & Williams, R. G. (2007). Meridional coherence of the North Atlantic meridional overturning circulation. *Geophysical Research Letters*, 34(23), L23606. <https://doi.org/10.1029/2007GL031731>
- Böning, C. W., Scheinert, M., Dengg, J., Biaostoch, A., & Funk, A. (2006). Decadal variability of subpolar gyre transport and its reverberation in the North Atlantic overturning. *Geophysical Research Letters*, 33(21), 1–5. <https://doi.org/10.1029/2006GL026906>
- Böning, C. W., Wagner, P., Handmann, P., Schwarzkopf, F. U., Getzlaff, K., & Biaostoch, A. (2023). Decadal changes in Atlantic overturning due to the excessive 1990s Labrador Sea convection. *Nature Communications*, 1–10. <https://doi.org/10.1038/s41467-023-40323-9>
- Buckley, M. W., Ferreira, D., Campin, J.-M., Marshall, J., & Tulloch, R. (2012). On the relationship between decadal buoyancy anomalies and variability of the Atlantic meridional overturning circulation. *Journal of Climate*, 25(23), 8009–8030. <https://doi.org/10.1175/JCLI-D-11-00505.1>
- Buckley, M. W., & Marshall, J. (2016). Observations, inferences, and mechanisms of the Atlantic meridional overturning circulation: A review. *Reviews of Geophysics*, 54(1), 5–63. <https://doi.org/10.1002/2015RG000493>
- Castruccio, F., Chang, P., Danabasoglu, G., Fu, D., Rosenbloom, N., Zhang, Q., et al. (2025). MESACLIP: A 500-year CESM HR pre-industrial control simulation forced with perpetual 1850 conditions. (Version 2025) [Dataset]. *Research Data Archive at the National Center for Atmospheric Research, Computational and Information Systems Laboratory*. <https://doi.org/10.5065/2K6J-SB78>
- Chang, P., Zhang, S., Danabasoglu, G., Yeager, S. G., Fu, H., Wang, H., et al. (2020). An unprecedented set of high-resolution earth system simulations for understanding multiscale interactions in climate variability and change. *Journal of Advances in Modeling Earth Systems*, 12(12), e2020MS002298. <https://doi.org/10.1029/2020MS002298>
- Chomiak, L. N., Yashayaev, I., Volkov, D. L., Schmid, C., & Hooper, J. A. (2022). Inferring advective timescales and overturning pathways of the deep western boundary current in the North Atlantic through Labrador Sea water advection. *Journal of Geophysical Research: Oceans*, 127(12), 1–23. <https://doi.org/10.1029/2022JC018892>
- Curry, R. G., McCartney, M. S., & Joyce, T. M. (1998). Linking subtropical deep water climate signals to North Atlantic subpolar convection variability. *Nature*, 391, 575–577.
- Danabasoglu, G. (2008). On multidecadal variability of the Atlantic meridional overturning circulation in the community climate system model version 3. *Journal of Climate*, 21(21), 5524–5544. <https://doi.org/10.1175/2008JCLI2019.1>
- Danabasoglu, G., Yeager, S. G., Kwon, Y.-O., Tribbia, J. J., Phillips, A. S., & Hurrell, J. W. (2012). Variability of the Atlantic meridional overturning circulation in CCSM4. *Journal of Climate*, 25(15), 5153–5172. <https://doi.org/10.1175/JCLI-D-11-00463.1>
- Deser, C., Alexander, M. A., Xie, S., & Phillips, A. S. (2009). Sea surface temperature variability: Patterns and mechanisms. *Annual Review of Marine Science*, 2(1), 115–143. <https://doi.org/10.1146/annurev-marine-120408-151453>
- Eden, C., & Willebrand, J. (2001). Mechanism of interannual to decadal variability of the North Atlantic circulation. *Journal of Climate*, 14(10), 2266–2280. [https://doi.org/10.1175/1520-0442\(2001\)014<2266:MOITDV>2.0.CO;2](https://doi.org/10.1175/1520-0442(2001)014<2266:MOITDV>2.0.CO;2)

- Famooss Paolini, L., Athanasiadis, P. J., Ruggieri, P., & Bellucci, A. (2022). The atmospheric response to meridional shifts of the Gulf Stream SST front and its dependence on model resolution. *Journal of Climate*, 35(18), 6007–6030. <https://doi.org/10.1175/JCLI-D-21-0530.1>
- Frajka-Williams, E., Foukal, N., & Danabasoglu, G. (2023). Should AMOC observations continue: How and why? *Philosophical Transactions of the Royal Society A: Mathematical, Physical & Engineering Sciences*, 381(2262), 20220195. <https://doi.org/10.1098/rsta.2022.0195>
- Frajka-Williams, E., Meinen, C. S., Johns, W. E., Smeed, D. A., Duche, A., Lawrence, A. J., et al. (2016). Compensation between meridional flow components of the Atlantic MOC at 26°N. *Ocean Science*, 12(2), 481–493. <https://doi.org/10.5194/os-12-481-2016>
- Fraser, N. J., Fox, A. D., & Cunningham, S. A. (2025). Impact of Ekman pumping on the meridional coherence of the AMOC. *Geophysical Research Letters*, 52(1), e2024GL108846. <https://doi.org/10.1029/2024GL108846>
- Fu, Y., Lozier, M. S., Biló, T. C., Bower, A. S., Cunningham, S. A., Cyr, F., et al. (2023). Seasonality of the meridional overturning circulation in the subpolar North Atlantic. *Communications Earth & Environment*, 4(1), 181. <https://doi.org/10.1038/s43247-023-00848-9>
- Fu, Y., Lozier, M. S., Majumder, S., & Petit, T. (2024). Water mass transformation and its relationship with the overturning circulation in the eastern Subpolar North Atlantic. *Journal of Geophysical Research: Oceans*, 129(12), e2024JC021222. <https://doi.org/10.1029/2024JC021222>
- Getzlaff, J., Böning, C. W., Eden, C., & Biastoch, A. (2005). Signal propagation related to the North Atlantic overturning. *Geophysical Research Letters*, 32(9), 1–4. <https://doi.org/10.1029/2004GL021002>
- Haarsma, R. J., Roberts, M. J., Vidale, P. L., Senior, C. A., Bellucci, A., Bao, Q., et al. (2016). High resolution model Intercomparison project (HighResMIP v1.0) for CMIP6. *Geoscientific Model Development*, 9(11), 4185–4208. <https://doi.org/10.5194/gmd-9-4185-2016>
- Hirschi, J., & Marotzke, J. (2007). Reconstructing the meridional overturning circulation from boundary densities and the zonal wind stress. *Journal of Physical Oceanography*, 37(3), 743–763. <https://doi.org/10.1175/JPO3019.1>
- Hodson, D. L. R., & Sutton, R. T. (2012). The impact of resolution on the adjustment and decadal variability of the Atlantic meridional overturning circulation in a coupled climate model. *Climate Dynamics*, 39(12), 3057–3073. <https://doi.org/10.1007/s00382-012-1309-0>
- Jackson, L. C., Biastoch, A., Buckley, M. W., Desbruyères, D. G., Frajka-Williams, E., Moat, B., & Robson, J. (2022). The evolution of the North Atlantic meridional overturning circulation since 1980. *Nature Reviews Earth & Environment*, 3(4), 241–254. <https://doi.org/10.1038/s43017-022-00263-2>
- Jackson, L. C., Peterson, K. A., Roberts, C. D., & Wood, R. A. (2016). Recent slowing of Atlantic overturning circulation as a recovery from earlier strengthening. *Nature Geoscience*, 9(7), 1–6. <https://doi.org/10.1038/ngeo2715>
- Johns, W. E., Elipot, S., Smeed, D. A., Moat, B., King, B., Volkov, D. L., & Smith, R. H. (2023). Towards two decades of Atlantic Ocean mass and heat transports at 26.5°N. *Philosophical transactions. Series A, Mathematical, Physical, and Engineering Sciences*, 381(2262), 20220188. <https://doi.org/10.1098/rsta.2022.0188>
- Johnson, H. L., Cessi, P., Marshall, D. P., Schloesser, F., & Spall, M. A. (2019). Recent contributions of theory to our understanding of the Atlantic meridional overturning circulation. *Journal of Geophysical Research: Oceans*, 124(8), 5376–5399. <https://doi.org/10.1029/2019JC015330>
- Khatri, H., Williams, R. G., Woollings, T., & Smith, D. M. (2022). Fast and slow subpolar ocean responses to the North Atlantic Oscillation: Thermal and dynamical changes. *Geophysical Research Letters*, 49(24), e2022GL101480. <https://doi.org/10.1029/2022GL101480>
- Kostov, Y., Johnson, H. L., Marshall, D. P., Heimbach, P., Forget, G., Holliday, N. P., et al. (2021). Distinct sources of interannual subtropical and subpolar Atlantic overturning variability. *Nature Geoscience*, 14(July), 491–495. <https://doi.org/10.1038/s41561-021-00759-4>
- Kostov, Y., Messias, M.-J., Mercier, H., Johnson, H. L., & Marshall, D. P. (2022). Fast mechanisms linking the Labrador Sea with subtropical Atlantic overturning. *Climate Dynamics*, 60(9–10), 2687–2712. <https://doi.org/10.1007/s00382-022-06459-y>
- Kwon, Y.-O., & Frankignoul, C. (2014). Mechanisms of multidecadal Atlantic meridional overturning circulation variability diagnosed in depth versus density space. *Journal of Climate*, 27(24), 9359–9376. <https://doi.org/10.1175/JCLI-D-14-00228.1>
- Lozier, M. S., Li, F., Bacon, S., Bahr, F., Bower, A. S., Cunningham, S. A., et al. (2019). A sea change in our view of overturning in the subpolar North Atlantic. *Science*, 363(6426), 516–521. <https://doi.org/10.1126/science.aau6592>
- Malcolm, R. (2018). MOHC HadGEM3-GC31-HH model output prepared for CMIP6 HighResMIP control-1950 (Version 2020) [Dataset]. *Earth System Grid Federation*. <https://doi.org/10.22033/ESGF/CMIP6.5881>
- Markina, M. Y., Johnson, H. L., & Marshall, D. P. (2024). Response of Subpolar North Atlantic meridional overturning circulation to variability in surface winds on different timescales. *Journal of Physical Oceanography*, 54(9), 1871–1887. <https://doi.org/10.1175/JPO-D-23-0236.1>
- Marotzke, J., & Klinger, B. A. (2000). The dynamics of equatorially asymmetric thermohaline circulations. *Journal of Physical Oceanography*, 30(5), 955–970. [https://doi.org/10.1175/1520-0485\(2000\)030<0955:TDOEAT>2.0.CO;2](https://doi.org/10.1175/1520-0485(2000)030<0955:TDOEAT>2.0.CO;2)
- Marshall, D. P., & Johnson, H. L. (2013). Propagation of meridional circulation anomalies along western and eastern boundaries. *Journal of Physical Oceanography*, 43(12), 2699–2717. <https://doi.org/10.1175/JPO-D-13-0134.1>
- McCarthy, G. D., Smeed, D. A., Johns, W. E., Frajka-Williams, E., Moat, B. I., Rayner, D., et al. (2015). Measuring the Atlantic meridional overturning circulation at 26°N. *Progress in Oceanography*, 130, 91–111. <https://doi.org/10.1016/j.pocan.2014.10.006>
- Megann, A., Blaker, A., Josey, S., New, A., & Sinha, B. (2021). Mechanisms for late 20th and early 21st century decadal AMOC variability. *Journal of Geophysical Research: Oceans*, 126(12). <https://doi.org/10.1029/2021JC017865>
- Menary, M. B., Jackson, L. C., & Lozier, M. S. (2020). Reconciling the relationship between the AMOC and Labrador Sea in OSNAP observations and climate models. *Geophysical Research Letters*, 47(18), e2020GL089793. <https://doi.org/10.1029/2020GL089793>
- Petit, T., Lozier, M. S., Josey, S. A., & Cunningham, S. A. (2020). Atlantic deep water formation occurs primarily in the Iceland basin and Irminger Sea by local buoyancy forcing. *Geophysical Research Letters*, 47(22), 1–9. <https://doi.org/10.1029/2020GL091028>
- Petit, T., Lozier, M. S., Rühls, S., Handmann, P., & Biastoch, A. (2023). Propagation and transformation of upper North Atlantic deep water from the subpolar gyre to 26.5°N. *Journal of Geophysical Research: Oceans*, 128(8), 1–13. <https://doi.org/10.1029/2023JC019726>
- Petit, T., Robson, J., Ferreira, D., & Jackson, L. C. (2023). Understanding the sensitivity of the North Atlantic subpolar overturning in different resolution versions of HadGEM3-GC3.1. *Journal of Geophysical Research: Oceans*, 128(10), e2023JC019672. <https://doi.org/10.1029/2023JC019672>
- Polo, I., Robson, J., Sutton, R., & Balmaseda, M. A. (2014). The importance of wind and buoyancy forcing for the boundary density variations and the geostrophic component of the AMOC at 26°N. *Journal of Physical Oceanography*, 44(9), 2387–2408. <https://doi.org/10.1175/jpo-d-13-0264.1>
- Roberts, M. J., Baker, A., Blockley, E. W., Calvert, D., Coward, A., Hewitt, H. T., et al. (2019). Description of the resolution hierarchy of the global coupled HadGEM3-GC3.1 model as used in CMIP6 HighResMIP experiments. *Geoscientific Model Development*, 12(12), 4999–5028. <https://doi.org/10.5194/gmd-12-4999-2019>
- Roberts, M. J., Jackson, L. C., Roberts, C. D., Meccia, V., Docquier, D., Koenig, T., et al. (2020). Sensitivity of the Atlantic meridional overturning circulation to model resolution in CMIP6 HighResMIP simulations and implications for future changes. *Journal of Advances in Modeling Earth Systems*, 12(8), 1–22. <https://doi.org/10.1029/2019MS002014>
- Smeed, D. A., McCarthy, G. D., Cunningham, S. A., Frajka-Williams, E., Rayner, D., Johns, W. E., et al. (2014). Observed decline of the Atlantic meridional overturning circulation 2004–2012. *Ocean Science*, 10(1), 29–38. <https://doi.org/10.5194/os-10-29-2014>

- Thornton, H. E., Smith, D. M., Scaife, A. A., & Dunstone, N. J. (2023). Seasonal predictability of the East Atlantic pattern in late autumn and early winter. *Geophysical Research Letters*, 50(1), e2022GL100712. <https://doi.org/10.1029/2022gl100712>
- Xu, X., Chassignet, E. P., Johns, W. E., Schmitz, W. J., & Metzger, E. J. (2014). Intraseasonal to interannual variability of the Atlantic meridional overturning circulation from eddy-resolving simulations and observations. *Journal of Geophysical Research: Oceans*, 119(8), 5140–5159. <https://doi.org/10.1002/2014JC009994>
- Yeager, S. G., Castruccio, F., Chang, P., Danabasoglu, G., Maroon, E., Small, J., et al. (2021). An outsized role for the Labrador Sea in the multidecadal variability of the Atlantic overturning circulation. *Science Advances*, 7(41), 1–25. <https://doi.org/10.1126/sciadv.abh3592>
- Zhai, Y., Yang, J., Wan, X., & Zou, S. (2021). The eastern Atlantic basin pathway for the export of the North Atlantic deep waters. *Geophysical Research Letters*, 48(24), 1–10. <https://doi.org/10.1029/2021GL095615>
- Zou, S., Lozier, M. S., & Xu, X. (2020). Latitudinal structure of the meridional overturning circulation variability on interannual to decadal time scales in the North Atlantic Ocean. *Journal of Climate*, 33(9), 3845–3862. <https://doi.org/10.1175/jcli-d-19-0215.1>

## References From the Supporting Information

- Le Bras, I. A.-A. (2023). Labrador Sea water spreading and the Atlantic meridional overturning circulation. *Philosophical Transactions of the Royal Society A: Mathematical, Physical & Engineering Sciences*, 381(2262), 20220189. <https://doi.org/10.1098/rsta.2022.0189>
- Wett, S., Rhein, M., Kieke, D., Mertens, C., & Moritz, M. (2023). Meridional connectivity of a 25-year observational AMOC record at 47°N. *Geophysical Research Letters*, 50(16), e2023GL103284. <https://doi.org/10.1029/2023GL103284>
- Willis, J. K. (2010). Can in situ floats and satellite altimeters detect long-term changes in Atlantic Ocean overturning? *Geophysical Research Letters*, 37(6), L06602. <https://doi.org/10.1029/2010GL042372>